Early stages of diamond growth on substrates with different carbon diffusivity

F. Inzoli[a,b,1], D. Dellasega[a,b], V. Russo[a], F. Ghezzi[b] and M. Passoni[a,b]

[a]*Dipartimento di Energia, Politecnico di Milano, via Ponzio 34/3, Milano 20133, Italy*

[b]*IFP, CNR, via R. Cozzi 53, Milano 20125, Italy*

Abstract

In this work, nanocrystalline diamond was deposited with a direct-current micro-plasma device on substrates with different carbon diffusivity. No substrate pre-treatment was performed and the same deposition conditions were adopted for all substrates, with the intention to investigate the first stages of growth. Samples were grown with increasing deposition time. Scanning electron microscopy and visible Raman spectroscopy were used to derive morphological and structural information. The growth dynamics was found to be the same on all substrates, with the deposition of a graphite layer prior to diamond growth. This layer was extensively characterized and a link between the structure and morphology of this layer and the subsequent features of the diamond grown on it was found. Moreover, diamond tens of micrometers thick was deposited in few hours, opening the possibility of producing diamond samples of practical interest. Particularly, the growth of nanocrystalline diamond on iron without substrate pre-treatment or interlayer deposition is reported, showing the feasibility of depositing diamond even on ferrous materials.

1. Introduction

Due to its outstanding properties, diamond possible applications broadened in many fields beyond the luxury industry [1–3]. This led to an increased global interest for diamond laboratory synthesis, with the aim to find out the main influencing parameters governing the deposition process and produce a valuable material. Chemical vapor deposition (CVD) techniques are

[1] *Corresponding author.*
E-mail address: federica.inzoli@polimi.it

nowadays the main industrial processes exploited to obtain synthetic diamond [4–6], especially at a laboratory scale. In particular, plasma-enhanced chemical vapor deposition (PECVD) techniques attract great interest because of the high growth rate and chemical purity of the deposited material [7]. Both single-crystal and polycrystalline diamond films can be produced: particularly, polycrystalline films have several interesting properties and less requirements on technical aspects related to the deposition process with respect to the single-crystal one. Moreover, the possibility to produce diamond in the form of coating preserving bulk diamond properties pushed forward the research of diamond laboratory synthesis.

Nevertheless, many difficulties afflict diamond films synthesis. One of the main difficulties derives from the choice of the substrate material. The possibility to grow diamond films on different substrates would be of interest for several applications, e.g. high power electronic, high frequency devices, UV-Vis-IR windows, wear resistance coatings and solid state detectors. However, having a high surface energy with respect to other materials, growing diamond on substrates different from diamond itself is anything but trivial [8]. Substrate materials suitable for diamond growth can be organized into three main families, depending on carbon/surface interaction and carbon diffusivity, namely [9,10]: materials having a little or no solubility or reaction with C, e.g. copper, silver and gold, materials in which carbon easily diffuses or dissolves or with a weak carbide formation, e.g. platinum, palladium, rhodium, nickel and iron, and materials with strong carbide-formation tendency, e.g. titanium, molybdenum, tungsten and silicon. Moreover, it is widely believed that nucleation of diamond on non-diamond substrates usually occurs via an intermediate non-diamond based layer [11,12]. This layer may be the result of the interaction with the substrate during the deposition process, since carbon atoms from the plasma can diffuse in the substrate material, saturate it and then act as preferential nucleation sites. To date, diamond films have been grown on carbide layer [13,14], graphite [15,16], diamond-like amorphous carbon and carbon oil [17–19]. Even if the theory of diamond growth mechanism is nowadays widely agreed, several contrasting observations on what happens in the nucleation phase on substrates even of the same family can be found in literature. For instance, both graphite, amorphous carbon and carbide compounds have been identified as the main responsible for diamond nucleation on carbide-forming materials [17,20,21]. In addition, substrate pre-treatments such as scratching, biasing or substrate coating are often used in order to enhance diamond nucleation density, and to control the grown morphology, texture and quality of the diamond films [22–24].

In a previous work [25], the authors already showed how the deposition of nanocrystalline diamond with a peculiar PECVD technique, i.e. the direct-current micro-plasma device (DC-μP),

on carbide-forming substrates such as silicon (Si) and molybdenum (Mo), proceeds towards the formation of an intermediate graphite layer. An explanation of the diamond growth dynamics in the early stages of the deposition has been provided, in accordance to diamond growth mechanism. Considering these results, a natural development is to extend the investigation to other family of substrates where other mechanisms of growing could be invoked to explain the diamond growing.

In this work, nanocrystalline diamond films have been grown on different substrate materials, with the same deposition apparatus and process conditions found in [25]. With the intention to deeply investigate the growth dynamics especially in the early stages of growth, materials with a diffusivity with carbon different from the case of Si and Mo were chosen. Tungsten (W), iron (Fe), nickel (Ni) and rhodium (Rh) were used in this work. W was chosen, because of its carburizing tendency as Mo and Si, but with a lower value of the Gibbs free energy of formation of the respective carbide [26]. Ni and Fe because of their high diffusivity with carbon. Moreover, even if both Ni and Fe have a carbide form, at the pressure and temperature deposition conditions used in [25], that are the same adopted for this work, no carbide compound should form [26]. Regarding Rh, the substrate used in this work is a 1 μm film of nanostructured columnar Rh grown with a pulsed laser deposition technique on Si [27]. Values of carbon diffusivity of the exploited substrates can be found in tab. 1, as derived from [7].

Substrate	Si	Mo	W	Fe	Ni
Carbon diffusivity [$cm^2\ s^{-1}$]	$7 \cdot 10^{-15}$	10^{-11}	10^{-13}	$8 \cdot 10^{-7}$	$2 \cdot 10^{-8}$

Tab. 1: Value of carbon diffusivity in different substrate materials, calculated at 800°C. For Rh, no available data are found.

The investigation of diamond growth was pursued depositing different spots with increasing deposition time. A characterization procedure similar to [25] combining SEM and Raman spectroscopy was adopted, whose potentiality has already been shown. Particularly, in the previous work a multi-wavelength Raman analysis has been performed, addressing structural information in an original and complete way. Since the aim of this work is to focus on what happens in the early stages, this time only visible Raman spectroscopy was used for structural characterization, and scanning electron microscopy (SEM) was used to derive the main morphological information about the grown samples.

2. Experimental technique

The deposition apparatus is schematically depicted in fig. 1.

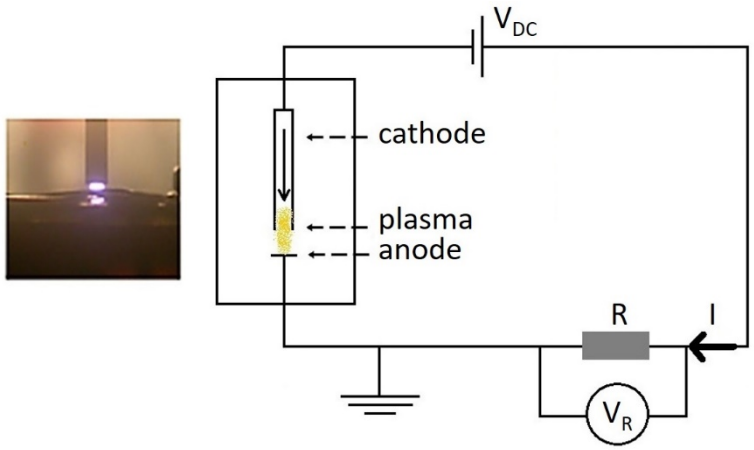

Fig. 1: Schematic representation of the direct-current micro-plasma device.

It consists of an in-house designed vacuum chamber of stainless steel, a plasma generating system and a gas supply system. The main feature of this experimental set-up is the stainless-steel column with 178 μm inner diameter capillary tube, acting as the micro-hollow cathode allowing the gas inlet used to create the flow-stabilized micro-plasma jet. All technical aspects related to such device and its configuration have already been addressed in [25]. The carbon source is methane gas mixed with hydrogen, with fluxes of 0.5 sccm and 100 sccm respectively. Substrates are previously cleaned with a sonic bath in hexane and deionized water, then placed under vacuum in the deposition chamber for several hours. No substrate pre-treatment is performed. Diamond was grown on all substrates increasing time from few minutes to hours. The deposition conditions are summarized in tab. 2 and tab. 3.

SEM micrographs are taken using a ZEISS Supra 40 scanning electron microscope with an accelerating voltage of 5 kV. Visible Raman spectroscopy is performed at room temperature by a Renishaw InVia micro-Raman spectrometer equipped with an Ar laser, using the blue line (457 nm, 2.71 eV). The spectral resolution is about 3 cm^{-1}.

Substrates	Mo, Si, W, Ni, Fe, Rh
Temperature	960 °C
Pressure	200 torr
Φ_{CH4}/Φ_{H2}	0.005
Supply voltage	610 V
Plasma current	10-12 mA

Tab. 2: Range of operating conditions for diamond deposition with DC-μP.

Substrates	Deposition time
Mo	2.5 min, 5 min, 10 min, 15 min, 30 min
Si	7 min, 15 min, 30 min, 1 hour, 2 hours
W	5 min, 15 min, 30 min, 1 hour
Ni	5 min, 15 min, 30 min, 1 hour
Fe	5 min, 15 min, 30 min, 1 hour
Rh	5 min, 15 min, 30 min, 1 hour

Tab. 3: Substrates used for diamond deposition and deposition times.

3. Results and discussion

All samples were grown with increasing deposition time, from few minutes to hours. SEM and Raman measurements were performed for all deposition times, and many similarities were found on all substrates, as in the previous work [25]: small and isolated agglomerates with different geometrical shapes are found in the first minutes, that grow both in dimensions and numbers as the deposition time increases, until coalescence in a nearly homogeneous deposition. Raman spectra change shape as the deposition time increases, showing a predominant graphitic signal for the early minutes of growth that disappears as the agglomerates coalesce in a continuous deposit, and at this point typical features on nanocrystalline diamond are found. In the following, only samples grown at 5 minutes and 30 minutes are shown. Particularly, 5 minutes were chosen because illustrative of the early stages of growth. 30 minutes were chosen since, as shown in the following, at this time a nearly homogeneous deposit was found on almost all substrates.

SEM images of the depositions on Mo, Si, W, Ni, Fe and Rh are shown in fig. 2, for the same process conditions. The deposition time was 5 minutes (with the only exception of Si, for which time was set at 7 minutes, since below this time nothing was found within SEM resolution). Results regarding Mo and Si substrates are referred to a previous work [25], but since one of the intention is to show what happens on substrate materials with different carbon diffusivity and belonging to different “families”, they will be recalled in the following together with results deriving from the new substrate materials.

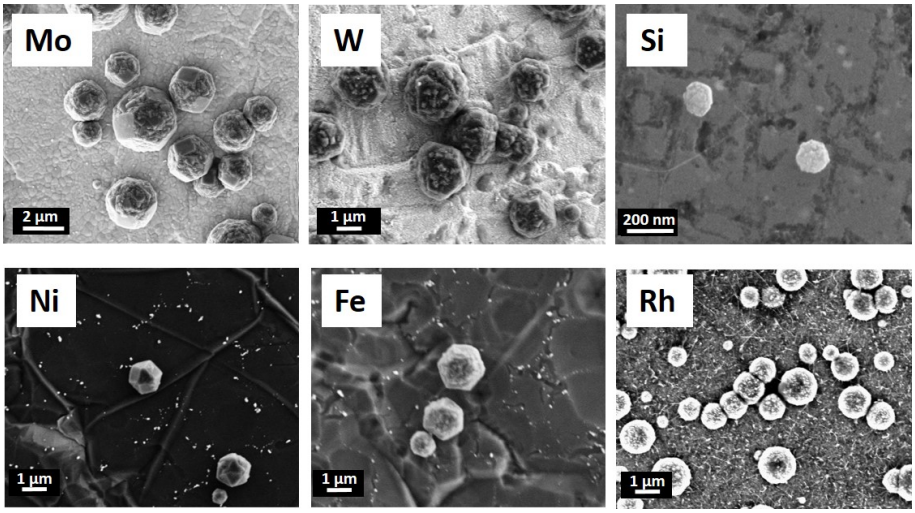

Fig. 2: SEM images of diamond deposited for few minutes on different substrates.

On all substrates, few and isolated agglomerates can be seen, with a well-faceted morphology but different dimensions, namely around 2 – 3 µm on Mo and W, slightly smaller and around 1 µm on Ni, Fe and Rh, and around 100 – 200 nm on Si. Raman spectra of these samples are shown in fig. 3.

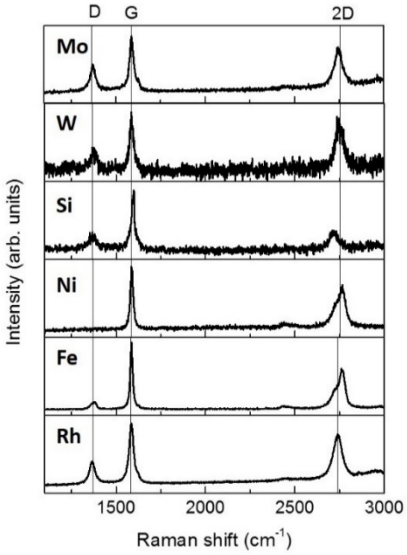

Fig. 3: Raman spectra of diamond deposited for few minutes on several substrates.

No diamond signal is detected at this grown time, even if the resolution of the instrument used allowed to take measurements directly on the agglomerates shown with SEM images: this result can be a combined effect of the scarce amount of diamond phase and the laser wavelength used to excite (since sp^3 has a resonant behaviour with the UV laser wavelength). Additionally, all spectra show typical features of graphitic films with a G peak at 1582 cm^{-1} and a D peak, related to disorder, at 1370 cm^{-1} (as expected using excitation at λ = 457 nm), except for Ni substrate

where no D peak is found. From the analysis of this peaks it is possible to characterize defectivity of the layers in graphitic materials [28], see below. The third Raman feature found at about 2740 cm^{-1} is the graphite second order peak, known as 2D peak, whose properties are related to the number and the stacking order of graphitic layers [29–31]. For instance, for the peculiar case of monolayer graphene, the 2D peak presents a single-Lorentzian shape at 2720 cm^{-1} (when using is λ = 457 nm), about 24 cm^{-1} wide and with higher intensity than the G peak. Increasing the number of layers, the 2D peak undergoes modifications relative to shape, position, width and intensity, depending on the stacking order among the layers. The split in two distinct components is the signature of crystalline graphite with Bernal stacking order (i.e. ABA stacking of layers), while for turbostratic graphite, in which the layers are randomly oriented, the 2D peak still has a single-Lorentzian shape, as in the case of monolayer graphene, but with a reduced intensity and a large width (up to 100 cm^{-1}). In any case a quantitative analysis is necessary to determine the number of layers [29–31], where the accepted nomenclature [32] refers to Few-Layer Graphene or FLG when the number of layers is between 2 and 5, Multi-Layer Graphene or MLG up to 10 layers, graphite for more than 10 layers. However, the nature of the graphitic film appears to be different from substrate to substrate. Qualitatively, for the case of Ni and Fe a double 2D peak reveals a Bernal stacking order, while a single Lorentzian 2D peak for all the other substrates suggests a misoriented stacking of graphitic layers [29]. In addition, in tab. 4 we report quantitative fitting data (position and width of the peak and relevant intensity ratio of peaks, calculated using the area of the fitting curves) that allow to better analyse the properties of the films.

Substrates	**Pos G (cm^{-1})**	**FWHM G (cm^{-1})**	**Pos D (cm^{-1})**	**FWHM D (cm^{-1})**	**Pos 2D (cm^{-1})**	**FWHM 2D (cm^{-1})**	**I_D / I_G**	**I_{2D} / I_G**	**Summary**
Mo	1588.5	28.6	1372.2	38.4	2745.3	56	0.64	1.38	MLG
Si	1595.3	22.4	1368.4	61.6	2718.2	56.7	0.58	0.74	TG
W	1586.6	21.2	1372.1	28.5	2749.4	51.9	0.41	1.96	FLG
Rh	1585.6	29.5	1366.4	35.5	2739.9	57.5	0.46	1.45	MLG
Fe	1586.1	15.8	1374.5	35.1	2725.3 / 2765.5	52.3 / 34.7	0.24	-	G
Ni	1587.5	18.3	0	0	2730.7 / 2767.5	56.7 / 37.7	0	-	G

Tab. 4: Peak properties of the Raman spectra of Fig. 3. For the case of Fe and Ni, where the 2D peak clearly presents two contributions, the I_{2D}/I_G ratio is not meaningful. In the last column, a summary of the type of graphitic material found on the substrates is reported (see text), where MLG, FLG, TG and G stand for multilayer graphene, few layer graphene, turbostratic graphite and graphite respectively.

First, analysing G and D peaks, information about the quality of the graphitic layers can be inferred. A general observation regards the position of the G peak, for all cases slightly higher than the expected 1582 cm^{-1}, probably due to interaction with the substrate (stress, induced doping). Further the G width is slightly broaden indicating the presence of some amount of disorder, except on Fe and Ni substrates, where values close to crystalline graphite are found, see fig. 4. The intensity ratio I_D / I_G, also reported in fig. 4, largely used in the carbon community to evaluate the defectivity of the layers [27], confirms this trend, being very small or zero for Fe and Ni substrates. Additionally, for these two substrates we observe a double 2D peak, as expected for Bernal stacked graphite. In the end, it appears that on substrates such as Ni and Fe the grown graphitic material shows a better crystallinity with respect to the other investigated substrates, all belonging to the "carburizing family" (i.e. Mo, Si and W). For them the previous observation of misoriented stacking of graphitic layers can be completed by the quantitative analysis of the single Lorentzian 2D peak, namely of its width and intensity ratio with the G peak, both reported in fig. 5. From the indication in the literature concerning these two parameters [28-30], we may conclude that on W a FLG is formed, on Mo and Rh a MLG, while several layers are present on Si. Moreover, on Rh, which is the only substrate with a columnar nanostructure, the multilayer system appears to be disordered than in the case of Mo, and this can be linked to the peculiar structure of the substrate.

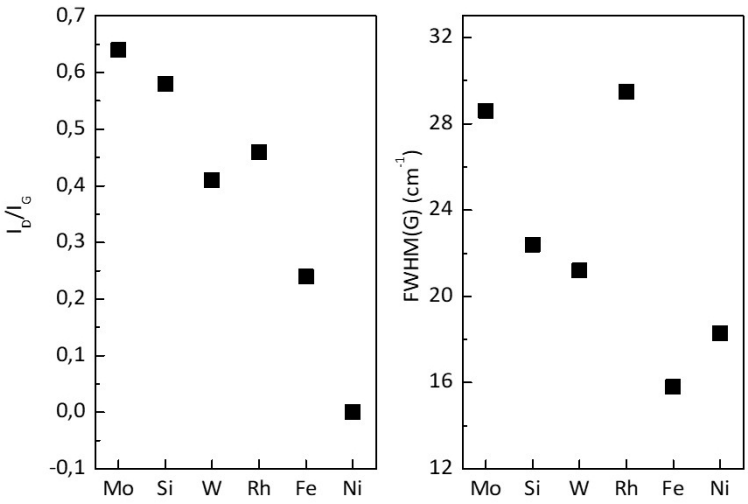

Fig. 4: I_D/I_G values and FWHM of the G peak derived from the fit of the spectra in fig. 3.

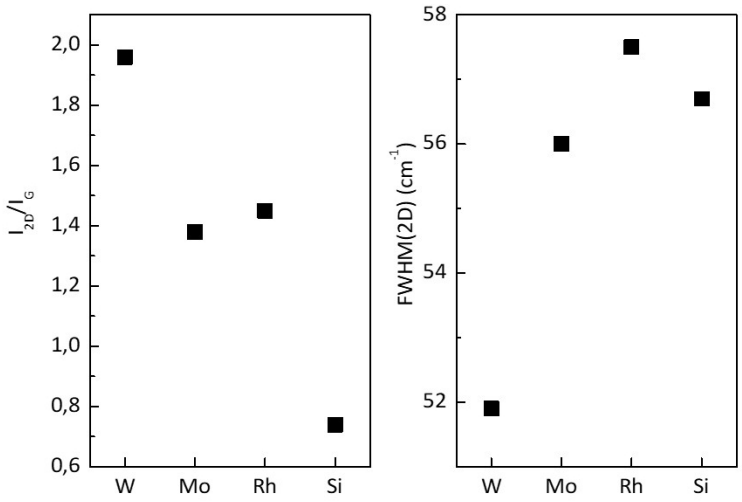

Fig. 5: I_{2D}/I_G values and FWHM of the 2D peak derived from the fit of the spectra in fig. 3, only for single Lorentzian 2D peak, which explains the absence of Fe and Ni. A different sequence of substrates is adopted with respect to the fig. 4.

From the spectra in fig. 3 we conclude that there is always a graphitic layer prior to diamond growth on all the investigated substrates, despite the carburizing or non-carburizing tendency. The diamond growth model is the one already theorized by Piekarczyk [33–37] based on three reaction steps that, with an appropriate thermodynamic formulation applied for diamond deposition with the DC-μP [38], appears to be suitable for justifying the formation of this graphitic layer. The main interesting result is how this model appears to stand for every kind of substrate used, despite the interaction channels that are supposed to happen depending on the carbon – substrate interaction.

SEM images and Raman spectra of diamond deposited on all these substrates for 30 minutes are shown in fig. 6 and fig. 7, respectively.

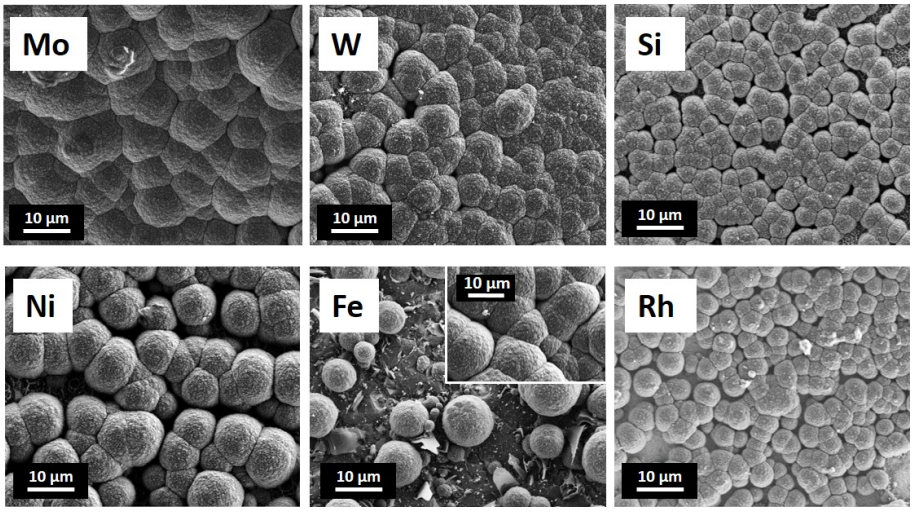

Fig. 6: SEM images of diamond deposited for 30 minutes on different substrates. For the case of Fe, in the inset is shown a deposit of 1 hour.

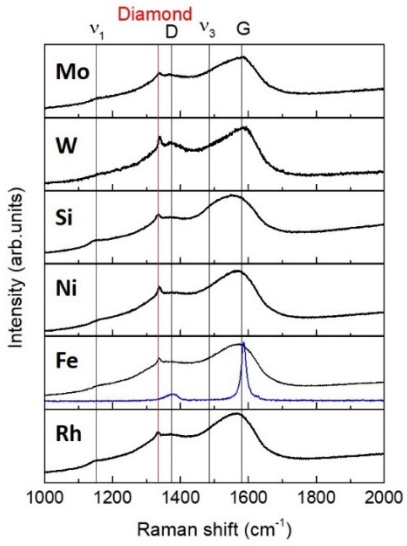

Fig. 7: Raman spectra of diamond deposited for 30 minutes on several substrates.

From SEM images, a nearly continuous deposition was found on all substrates, with a diameter around 200 – 300 µm, with exception of Fe, where few, isolated aggregates are visible. However, for 1 hour of deposition a continuous deposit with ballas-like morphology was found even on Fe and no delamination occurred after substrate cooling. This observation is significant for the specific case of iron, since Fe-based materials are extensively considered non-ideal substrates for direct coating of diamond without the deposition of an appropriate interfacial layer with the aim of increasing diamond adhesion and preventing its peeling off after cooling; Fe has indeed a catalytic behaviour with respect to sp^2 formation, and this is worsened by the high diffusivity that carbon has in this material, leading the formation of cluster of critical size for diamond nucleation difficult and long-time [39–43]. In the literature some positive results have been conversely

reported on stainless steel, where problems in diamond growth on ferrous materials such as the surface graphitization, long incubation time, substrate softening and poor adhesion were overcome without the need of interfacial layer but with a low temperature deposition process [44]. Considerably, in this work no interlayer deposition is intentionally performed on Fe previously to diamond deposition, and the process temperature used is in the usually employed range for diamond deposition with PECVD. Therefore, the spontaneous formation of a graphitic interlayer during our process, common to all substrates, is crucial for diamond growth on Fe. On Rh, diamond was grown for the first time and with a nucleation density and kinetics not far from that of the carburizing materials. In the Raman spectra (see fig. 7), typical nanocrystalline diamond features are found on all substrates. The diamond peak at 1332 cm^{-1} confirms the presence of sp^3 crystalline phase, whereas the D and G features are related to the disordered sp^2 content, always present at the grain boundaries. Also, peaks assigned to nanocrystalline diamond are found, i.e. v_1 and v_3, due to the *trans-polyacetylene* content that characterizes nanocrystalline diamond grain boundaries. This results agree with the ball-shape morphology highlighted by SEM characterization (see fig. 6). For the case of Fe, which is the only one at 30 minutes where the diamond agglomerates still are not coalescent, Raman measurement directly on the substrate around the agglomerates was possible: the result is the blue spectrum (see fig. 7), that again confirms the presence of the graphitic system under the diamond agglomerates. The evident difference in morphology between the well-faceted agglomerates of the first minutes of growth and the nanocrystalline diamond obtained for prolonged deposition time, can be attributed to a change in the growth mechanism as diamond particles reach a certain critical size, i.e. from a layer-by-layer growth to a normal growth [45].

In order to characterize diamond deposited at 30 minutes on all substrates, Raman spectra of fig. 7 were all fitted, following a precise procedure that has already been extensively justified in [25]: a single Lorentzian function were used for the diamond peak, while four Gaussians were used to fit the v_1, v_3, D and G peaks. Consequently, information regarding the diamond peak position and FWHM were acquired: the values of these features are strongly linked to diamond stress state and crystallinity, respectively. Moreover, a qualitative evaluation of sp^3/sp^2 content was performed, using the experimental coefficient *f* already described in [25]. The diamond peak position and FWHM values are reported in tab. 8, together with the trend of the coefficient *f*.

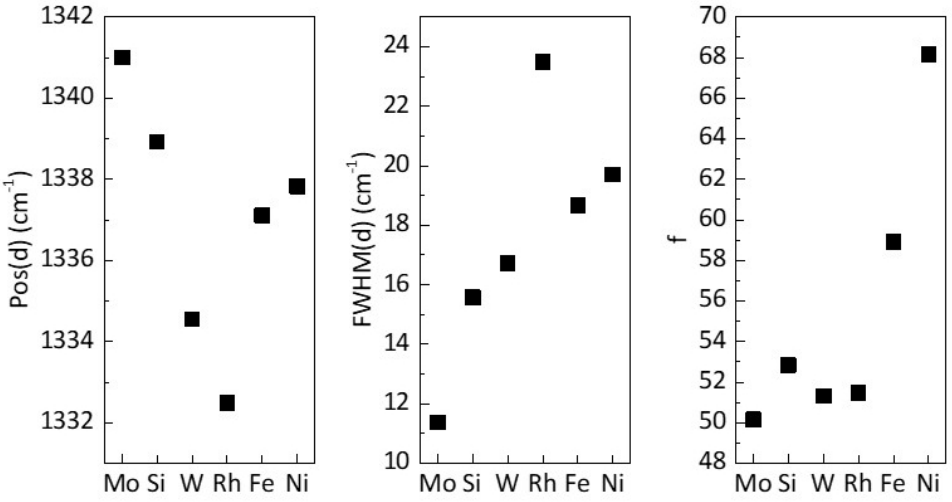

Fig. 8: Values of the d peak position, FWHM and of the f coefficient as derived from the fitting of Raman spectra of fig. 7.

The slight shift in the diamond peak with respect to its theoretical position is symptomatic of stress states probably due to the substrate-diamond lattice mismatch, whereas the FWHM values are likely to be in the range of values of diamond with small grain sizes. Being the f coefficient linked to the sp^3/sp^2 content, a low value of this coefficient is symptomatic of diamond with a smaller grain size, since the sp^2 is located mainly at the grain boundaries. Considering this, some observations can be derived. On Rh coated silicon, the d peak position is centred in its theoretical value, and thus a relaxation of the interface stresses can be deduced. At the same time, the high value of FWHM signifies a diamond with a very small grain size and low crystallinity, which is in accordance with the low value of the f coefficient. It is interesting to note that the sub-micrometric Rh film despite its small thickness determines the features of the growing diamond like the other bulk metal substrates. Additionally, the nanocrystalline phase of the deposited diamond is probably influenced by the nanostructured columnar nature of the Rh film. On Fe and Ni, that show similar values of all diamond features, the f factor is the higher among the analysed substrates: this can find an explanation in the fact that on both substrates a crystalline graphite if found in the early stages of growth. Indeed, nucleation of diamond on graphite precursors is supposed to happen easily, supported by both experimental and theoretical observations [15,16,20]: this implies that when the precursor is a well-ordered graphite rather than a systems composed by randomly oriented multilayer, diamond tends to grow easily, and with a higher content with sp^3 phase with respect to sp^2, and thus a higher grain size. On Mo, Si and W instead, where a multilayer system is found in the early stages of growth, diamond still grow but with a lower grain size (low sp^3/sp^2 content); at the same time, the crystallinity of this grain size is better (see FWHM values) than on the other substrates. In summary, the increasing in sp^3/sp^2 content (and thus in the grain dimension) we observed is linked to the crystallinity of the early stages

graphite, and this is clearly shown in fig. 9., where the dependence of the f factor of diamond on the I_D/I_G ratio of graphite is reported.

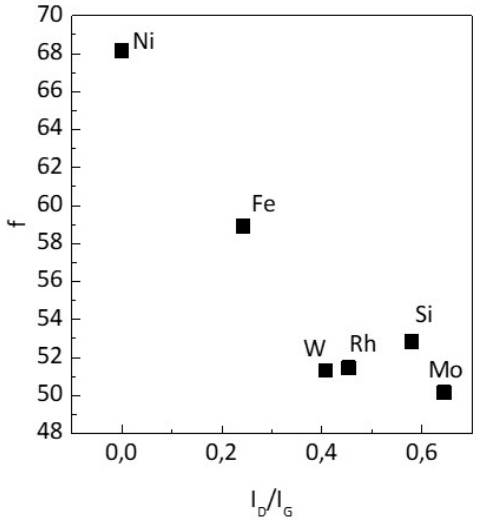

Fig. 9: sp^3/sp^2 content (and grain dimension) of diamond as a function of the graphite crystallinity.

Finally, exploiting the extreme smoothness and flatness of Si substrate, thickness and deposition area of samples grown for 90 minutes, 3 hours and 5 hours were measured and are listed in tab 5. As an example, SEM cross-section and top view of the sample deposited at 90 minutes are shown in fig. 10.

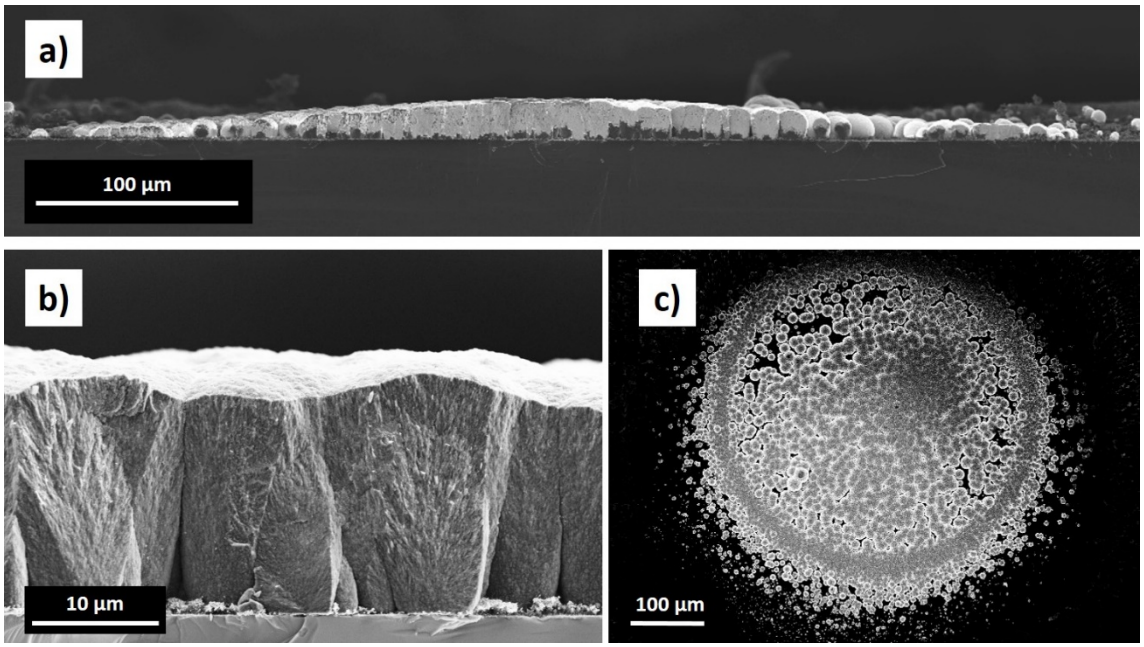

Fig. 10 Diamond grown on Si for 90 minutes: a) a cross-section of the sample, b) a magnification of the cross-section in the centre of the deposit and c) a top view of the deposit.

Growth time	90 min	3 hours	5 hours
Area [mm^2]	≈ 0,19	≈ 0,22	≈ 0,28
Thickness [μm]	20	40	90

Tab. 5: Superficial areas and thicknesses of diamond deposited on Si with increasing deposition time

The deposit shows a circular shape (see fig. 9.c), and a Gaussian-like profile (see fig. 9.a), with the density of agglomerates decreasing from the centre to the periphery region of the deposition. Nevertheless, it is worth noticing that, for higher thickness, the deposition results homogeneous over the whole area, and a higher covering is achieved, even if the plasma plume dimension is fixed at 178 μm. From cross-section view (see fig. 9.b), we clearly appreciate a columnar growth with diamond agglomerates starting coalescence after a thickness of few microns. From data reported in tab. 5, we note that the thickness is almost linear with deposition time, with a growth rate of about 16 μm/h.

4. Conclusions

In this work, nanocrystalline diamond was deposited on several substrate materials without substrate pre-treatment and with the same deposition conditions. Basing on the results, this work demonstrates definitively the extreme versatility of the direct-current micro-plasma device regarding the successful deposition of nanocrystalline diamond on various substrate materials. Of practical interest is the case on Fe, since diamond deposition on Fe-based materials has always been an arduous task. In this work, nanocrystalline diamond with good crystalline quality and high sp^3/sp^2 content was successfully deposited on Fe, opening the possibility of exploiting the DC-μP device for diamond deposition on stainless steel. Additionally, important similarities can be found in the dynamics of growth on all substrates, suggesting that the formation of a graphitic layer at the diamond-substrate interface is the driving force through diamond deposition with this peculiar technique. A detailed analysis shows that this graphitic layer can have different nature, depending on the substrate materials, ranging from few-layers graphene to graphite or turbostratic graphite. The initial graphitic layer is then responsible for the growth of nanocrystalline diamond with different features regarding the sp^3/sp^2 content and the grain crystallinity. Finally, samples grown on silicon for prolonged deposition time, together with the possibility to exploit the translating apparatus for dynamic depositions that equips the DC-μP device [25], show the

feasibility of tuning the dimension and thickness of the deposition to produce films of practical interest.

Bibliography

[1] P.W. May, Diamond thin films: a 21st-century material, Philos. Trans. R. Soc. Lond. Math. Phys. Eng. Sci. 358 (2000) 473–495. doi:10.1098/rsta.2000.0542.

[2] A. Gicquel, K. Hassouni, F. Silva, J. Achard, CVD diamond films: from growth to applications, Curr. Appl. Phys. 1 (2001) 479–496. doi:10.1016/S1567-1739(01)00061-X.

[3] D.M. Gruen, Nanocrystalline diamond films, Annu. Rev. Mater. Sci. 29 (1999) 211–259. doi:10.1146/annurev.matsci.29.1.211.

[4] P. Hess, The mechanical properties of various chemical vapor deposition diamond structures compared to the ideal single crystal, J. Appl. Phys. 111 (2012) 51101. doi:10.1063/1.3683544.

[5] S.-T. Lee, Z. Lin, X. Jiang, CVD diamond films: nucleation and growth, Mater. Sci. Eng. R Rep. 25 (1999) 123–154. doi:10.1016/S0927-796X(99)00003-0.

[6] J.C. Angus, Diamond synthesis by chemical vapor deposition: The early years, Diam. Relat. Mater. 49 (2014) 77–86. doi:10.1016/j.diamond.2014.08.004.

[7] H. Liu, D.S. Dandy, Studies on nucleation process in diamond CVD: an overview of recent developments, Diam. Relat. Mater. 4 (1995) 1173–1188. doi:10.1016/0925-9635(96)00297-2.

[8] W. Zhu, B.R. Stoner, B.E. Williams, J.T. Glass, Growth and characterization of diamond films on nondiamond substrates for electronic applications, Proc. IEEE. 79 (1991) 621–646. doi:10.1109/5.90129.

[9] D. Das, R.N. Singh, A review of nucleation, growth and low temperature synthesis of diamond thin films, Int. Mater. Rev. 52 (2007) 29–64. doi:10.1179/174328007X160245.

[10] J.J. Gracio, Q.H. Fan, J.C. Madaleno, Diamond growth by chemical vapour deposition, J. Phys. -Appl. Phys. 43 (2010) 374017. doi:10.1088/0022-3727/43/37/374017.

[11] M.C. Polo, J. Cifre, J. Esteve, Interfacial layer effects in the growth of CVD diamond, Diam. Relat. Mater. 3 (1994) 492–494. doi:10.1016/0925-9635(94)90209-7.

[12] H.M. Liu, D.S. Dandy, Nucleation kinetics of diamond on carbide-forming substrates during chemical vapor deposition .1. Transient nucleation stage, J. Electrochem. Soc. 143 (1996) 1104–1109. doi:10.1149/1.1836591.

[13] Y. Kato, M. Goto, R. Sato, K. Yamada, A. Koga, K. Teii, C. Srey, S. Tanaka, Formation of epitaxial 3C-SiC layers by microwave plasma-assisted carbonization, Surf. Coat. Technol. 206 (2011) 990–993. doi:10.1016/j.surfcoat.2011.04.021.

[14] F. Long, Q. Wei, Z.M. Yu, J. Luo, X. Zhang, H. Long, X. Wu, Effects of temperature and Mo2C layer on stress and structural properties in CVD diamond film grown on Mo foil, J. Alloys Compd. 579 (2013) 638–645. doi:10.1016/j.jallcom.2013.06.146.

[15] W.R.L. Lambrecht, C.H. Lee, B. Segall, J.C. Angus, Z. Li, M. Sunkara, Diamond nucleation by hydrogenation of the edges of graphitic precursors, Nature. 364 (1993) 607–610. doi:10.1038/364607a0.

[16] D.N. Belton, S.J. Schmieg, Nucleation of chemically vapor deposited diamond on platinum and nickel substrates, Thin Solid Films. 212 (1992) 68–80. doi:10.1016/0040-6090(92)90502-3.

[17] B.R. Stoner, G.-H.M. Ma, S.D. Wolter, J.T. Glass, Characterization of bias-enhanced nucleation of diamond on silicon by \textit{invacuo} surface analysis and transmission electron microscopy, Phys. Rev. B. 45 (1992) 11067–11084. doi:10.1103/PhysRevB.45.11067.

[18] A.A. Morrish, P.E. Pehrsson, Effects of surface pretreatments on nucleation and growth of diamond films on a variety of substrates, Appl. Phys. Lett. 59 (1991) 417–419. doi:10.1063/1.105448.
[19] J. Muller, F. Antoni, E. Fogarassy, F. Le Normand, HFCVD diamond nucleation and growth on DLC carbon films obtained by laser ablation, Carbon. 36 (1998) 565–568. doi:10.1016/S0008-6223(98)00067-0.
[20] M.M. Waite, S.I. Shah, X-ray photoelectron spectroscopy of initial stages of nucleation and growth of diamond thin films during plasma assisted chemical vapor deposition, Appl. Phys. Lett. 60 (1992) 2344–2346. doi:10.1063/1.107474.
[21] W.L. Wang, K.J. Liao, L. Fang, J. Esteve, M.C. Polo, Analysis of diamond nucleation on molybdenum by biased hot filament chemical vapor deposition, Diam. Relat. Mater. 10 (2001) 383–387. doi:10.1016/S0925-9635(00)00505-7.
[22] R. Shima-Edelstein, I. Gouzman, A. Hoffman, The influence of surface roughness and chemical modification of silicon surfaces on dc-glow discharge enhanced diamond nucleation, Carbon. 39 (2001) 337–342. doi:10.1016/S0008-6223(00)00108-1.
[23] R. Shima, Y. Chakk, A. Hoffman, Influence of Ti, Fe, and Cu metal submicron-particles on diamond CVD on Si substrates, Carbon. 38 (2000) 1839–1843. doi:10.1016/S0008-6223(00)00019-1.
[24] M.-J. Chiang, M.-H. Hon, X-ray photoelectron spectroscopy investigation of substrate surface pretreatments for diamond nucleation by microwave plasma chemical vapor deposition, J. Cryst. Growth. 211 (2000) 211–215. doi:10.1016/S0022-0248(99)00769-1.
[25] F. Inzoli, D. Dellasega, V. Russo, R. Caniello, C. Conti, F. Ghezzi, M. Passoni, Nanocrystalline diamond produced by direct current micro-plasma: Investigation of growth dynamics, Diam. Relat. Mater. 74 (2017) 212–221. doi:10.1016/j.diamond.2017.03.011.
[26] S.R. Shatynski, The thermochemistry of transition metal carbides, Oxid. Met. 13 (n.d.) 105–118. doi:10.1007/BF00611975.
[27] A. Uccello, D. Dellasega, S. Perissinotto, N. Lecis, M. Passoni, Nanostructured rhodium films for advanced mirrors produced by Pulsed Laser Deposition, J. Nucl. Mater. 432 (2013) 261–265. doi:10.1016/j.jnucmat.2012.08.046.
[28] M.A. Pimenta, G. Dresselhaus, M.S. Dresselhaus, L.G. Cançado, A. Jorio, R. Saito, Studying disorder in graphite-based systems by Raman spectroscopy, Phys. Chem. Chem. Phys. 9 (2007) 1276–1290. doi:10.1039/B613962K.
[29] M. Passoni, V. Russo, D. Dellasega, F. Causa, F. Ghezzi, D. Wolverson, C.E. Bottani, Raman spectroscopy of nonstacked graphene flakes produced by plasma microjet deposition, J. Raman Spectrosc. 43 (2012) 884–888. doi:10.1002/jrs.3111.
[30] L.M. Malard, M.A. Pimenta, G. Dresselhaus, M.S. Dresselhaus, Raman spectroscopy in graphene, Phys. Rep. 473 (2009) 51–87. doi:10.1016/j.physrep.2009.02.003.
[31] A. Reina, X. Jia, J. Ho, D. Nezich, H. Son, V. Bulovic, M.S. Dresselhaus, J. Kong, Large Area, Few-Layer Graphene Films on Arbitrary Substrates by Chemical Vapor Deposition, Nano Lett. 9 (2009) 30–35. doi:10.1021/nl801827v.
[32] A. Bianco, H.-M. Cheng, T. Enoki, Y. Gogotsi, R.H. Hurt, N. Koratkar, T. Kyotani, M. Monthioux, C.R. Park, J.M.D. Tascon, J. Zhang, All in the graphene family – A recommended nomenclature for two-dimensional carbon materials, Carbon. 65 (2013) 1–6. doi:10.1016/j.carbon.2013.08.038.
[33] W. Piekarczyk, Diamond Vapor Interface and Processes Proceeding on It During Growth of Diamond Crystals .1. Diamond (111) Face, J. Cryst. Growth. 119 (1992) 345–362. doi:10.1016/0022-0248(92)90690-K.
[34] W. Piekarczyk, How and why CVD diamond is formed: A solution of the thermodynamic paradox, J. Mater. Sci. 33 (1998) 3443–3453. doi:10.1023/A:1013214220026.
[35] W. Piekarczyk, Crystal growth of CVD diamond and some of its peculiarities, Cryst. Res. Technol. 34 (1999) 553–563. doi:10.1002/(SICI)1521-4079(199906)34:5/6<553::AID-CRAT553>3.0.CO;2-8.

[36] W. Piekarczyk, S. Prawer, Role of Atomic-Hydrogen in Preventing Surface Reconstruction and Sp(2) Bond Formation During Chemical-Vapor-Deposition of Diamond, Diam. Relat. Mater. 2 (1993) 41–47. doi:10.1016/0925-9635(93)90140-W.
[37] W. Piekarczyk, S. Prawer, Diamond-Vapor Interface and Processes Proceeding on It During Growth of Diamond Crystals .2. Diamond (011) Face, J. Cryst. Growth. 135 (1994) 172–182. doi:10.1016/0022-0248(94)90739-0.
[38] F. Ghezzi, G. Cacciamani, R. Caniello, D.C. Toncu, F. Causa, D. Dellasega, V. Russo, M. Passoni, Carbon Structures Grown by Direct Current Microplasma: Diamonds, Single-Wall Nanotubes, and Graphene, J. Phys. Chem. C. 118 (2014) 24714–24722. doi:10.1021/jp501440b.
[39] V. Kundrat, X. Zhang, K. Cooke, H. Sun, J. Sullivan, H. Ye, A novel Mo-W interlayer approach for CVD diamond deposition on steel, Aip Adv. 5 (2015) 47130. doi:10.1063/1.4918969.
[40] A.K. Sikder, T. Sharda, D.S. Misra, D. Chandrasekaram, P. Selvam, Chemical vapour deposition of diamond on stainless steel: the effect of Ni-diamond composite coated buffer layer, Diam. Relat. Mater. 7 (1998) 1010–1013. doi:10.1016/S0925-9635(99)80000-4.
[41] X. Sun, H.T. Ma, L.Z. Yang, M. Sanchez-Pasten, D. Craig Penner, Y.S. Li, Q. Yang, Metal dusting, carburization and diamond deposition on Fe–Cr alloys in CH4–H2 plasma atmospheres, Corros. Sci. 98 (2015) 619–625. doi:10.1016/j.corsci.2015.06.001.
[42] A. Fayer, O. Glozman, A. Hoffman, Deposition of Continuous and Well Adhering Diamond Films on Steel, Appl. Phys. Lett. 67 (1995) 2299–2301. doi:10.1063/1.115132.
[43] H. Chen, M. Nielsen, C. Gold, R. Dillon, J. Digregorio, T. Furtak, Growth of Diamond Films on Stainless-Steel, Thin Solid Films. 212 (1992) 169–172. doi:10.1016/0040-6090(92)90516-E.
[44] K. Tsugawa, S. Kawaki, M. Ishihara, M. Hasegawa, Direct Coating of Nanocrystalline Diamond on Steel, Jpn. J. Appl. Phys. 51 (2012) 90122. doi:10.1143/JJAP.51.090122.
[45] N.A. Feoktistov, S.A. Grudinkin, V.G. Golubev, M.A. Baranov, K.V. Bogdanov, S.A. Kukushkin, Evolution of the Morphology of Diamond Particles and Mechanism of Their Growth during the Synthesis by Chemical Vapor Deposition, Phys. Solid State. 57 (2015) 2184–2190. doi:10.1134/S1063783415110104.